Convective Building of a Pycnocline: Laboratory Experiments

David W. Pierce* and Peter B. Rhines

School of Oceanography, University of Washington, Seattle, Washington

Revised Version, May, 1994

*Present affiliation: Scripps Institution of Oceanography, University of California, San Diego.

Abstract

We examine the convective building of a pycnocline using a laboratory model forced by surface fluxes of saline water at one end and fresh water at the other. A deep recirculation evolves in the tank, which homogenizes the interior fluid by repeated passes through the dense, descending plume. A thin, fresh surface layer develops and modifies the effective buoyancy flux into the the dense plume, causing the interior velocities to fall to an intermediate-time minimum. Adding bottom topography under the dense source greatly reduces the amount of entrainment which the descending plume undergoes. In this case, the tank fills with a deep, heavy layer, which causes the plume to "lift off" the bottom of the tank and detrain at successively higher depths in the water column. A simple numerical "plume" model shows that this cannot be a steady state, as it is not in diffusive balance; the plume must eventually return to the bottom of the tank and ventilate the interior waters. Adding rotation increases the surface mixing, thickens the halocline, and increases the observed variability in the salinity field.

1. Introduction

There has been a great deal of laboratory work examining non-rotating convection from monopolar point sources, and convection in fluids forced on opposing surfaces, such as in classic Rayleigh-Bernard convection. There has been less work performed in a rotating frame of reference, although there has been a surge of interest in this area (Hopfinger et al., 1982; Fernando et al., 1989; Boubnov and Golitsyn, 1990; Fernando et al., 1991). There has, however, been little work done on systems forced by balanced *dipoles* of buoyancy flux on the same surface, although this is the case most relevant to the oceans and atmosphere; and even less on the rotating version (Hignett et al., 1981).

We describe here a series of laboratory experiments and a simple model examining the circulation and density fields evolved in a fluid forced by a dipole of buoyancy flux, with the buoyancy source and sink on the same surface (taken to be the top; all the results apply to the inverted case equally well, however). Our primary objectives were to determine the equilibrium density structure of the the dipole-forced system, determine what effect changes in bottom topography—via the mechanism of entrainment under the dense plume—have on the system, and evaluate the influence of rotation on the system's final state.

The physical archetype which we have in mind for this experiment is the Earth's thermohaline circulation. The relevant characteristics of the thermohaline circulation as far as this discussion goes are that it is forced primarily by surface buoyancy fluxes, with a geographical separation of extrema (heating at the equator, cooling at the poles) with a net flux of approximately zero. The climate is thus considered to be in steady state. This choice of physical process to examine dictates the general form of the forcing function to be used; one with a non-zero net forcing would be inappropriate, since we want to consider times long compared to the overturning time of the deep circulation, and wish to come to an approximate steady state. Similarly, one with forcing applied other than at the surface would not be appropriate, since on the Earth the overwhelming majority of the buoyancy forcing occurs at the surface. A dipole of surface buoyancy forcing was thus chosen as the simplest pattern which met these requirements.

In general, the presence of a *dipole* of forcing is crucial, as it allows the system to come to a non-trivial equilibrium state; by contrast, the system with monopolar forcing simply approaches the density of the source (for fixed-value boundary conditions) or continue to lighten or densify indefinitely (for fixed-flux boundary conditions). When a system is forced by a dipole, circulation pathways within the fluid must evolve which carry buoyancy from the source to the sink. In classical Bernard-Rayleigh convection, this circulation takes the form of vertically-oriented, overturning cells of various planforms (Chandrasekhar, 1953). However, when the system is forced with both the source and sink on the same geopotential surface, *horizontal* circulations must evolve to accomplish this density transfer. This is the essence of the ocean's deep thermohaline circulation.

Diffusion also plays an important, but different, role in the two systems. In Bernard-Rayleigh convection, the only way density can enter and exit the system is by diffusion across thin boundary layers adjacent to the forcing surfaces. In a system forced by a dipole from above, by contrast, a thin, light surface layer must necessarily be formed, and diffusion into this layer from below is important to setting up the final advective/diffusive balance. This arises because (for a top-forced system) fluid near the lightening source becomes lighter still and floats on the surface, remaining near the light source. Fluid near the densening source, by contrast, is rapidly pulled away from the formation region by gravity, and cannot densify further. This results in a characteristic population distribution of densities with a tiny amount of extremely light fluid, and a large mass of slightly heavy fluid.

The role of bottom topography and entrainment under a convecting plume is also of interest. There are regions of the ocean where convection proceeds into the interior without any apparent influence from topography, such as the Labrador Sea, and the Gulf of Lyons in the Mediterranean. There are other areas where convection is strongly influenced by topography, such as the overflows at the strait of Gibraltar, the Denmark straits, and the shelf processes in the Weddell Sea. The entrainment which a dense source experiences on the way to reaching a neutral level is strongly influenced by such topographic variations. In the laboratory experiments described here, we use an idealized bottom topography (a simple sloping plane with no lateral variation) to vary the entrainment which the dense plume experienced, and examined the effect this had on the interior velocity and density fields.

The orginazation of this paper is as follows. Section 2 describes the laboratory setup, and the instrumentation and measurement methods. Section 3 presents the results from the control case, as well as test cases with bottom topography and rotation. Section 4 describes the various time scales germane to the problem. Section 5 presents a "numerical plume model", used to examine the behavior of the system at times longer than possible in the laboratory setting. Section 6 is a brief discussion relating these results to oceanic observations, and Section 7 presents our conclusions.

a. Prior Work

Stommel [1962] speculated that the pattern of surface forcing of the ocean was irrelevant to the particular sites which would be chosen for deep convection. In particular, he thought that a linear surface temperature gradient would result in a single overturning cell, similar to that observed in the ocean. This idea was experimentally verified by Rossby [1965], who studied convection driven by a linear bottom temperature gradient in a tank .245 meters long by .10 meters tall by .075 meters thick. Rossby also systematically varied the viscosity of his test fluid, and demonstrated the effect which this had on the boundary layer which evolved.

Baines and Turner [1969] examined the way in which a monopolar source would fill a confined region in a non-rotating environment. The control case performed here could be viewed as an extension of that work to the case with a dipole of forcing, so that an interesting long-term equilibrium solution is approached. Additionally, one of the rotating runs was performed without a fresh source, and so can be considered the extension of that work to the rotating case.

2. Laboratory Setup

a. Physical configuration

Most of the experiments described here were performed in a tank .92 meters long by .16 meters tall by .045 meters wide. A schematic of the setup is shown in Figure 1.

We imagine that the experiments are a laboratory realization of the following, idealized system: a tank driven by dipole of buoyancy forcing, such that the surface fluid at one end of the tank is becoming denser, and the surface fluid at the other end is becoming lighter. We approach this idealization by carefully pumping highly saline water in at one end of the tank, and fresh water in at the other. The tubes through which the fluid was delivered were set to just come into contact with fluid's free surface, thereby avoiding any extraneous mixing effects arising from dripping the water into the tank. In the experiments shown here, the tank was initially filled with water of salinity halfway between the two sources. Typical values for the runs shown are an initial tank salinity of 5%, and forcing of 10% at one end and 0% salinity at the other. With a 5% salinity difference, the flow rate into the tank is equivalent to a buoyancy flux of 2.6×10^{-8} m^4/sec^3.

The flux of fluid pumped into the tank is small—a total (from both sources) of about 0.15 ml/sec. To maintain a constant volume of fluid in the tank over time, is is necessary to remove this same amount. We accomplished this by using an eight-channel peristaltic pump. Four of the channels were devoted to pumping fluid into the tank; two delivered saline water and two delivered fresh water, while the other four channels pumped fluid out of the tank at approximately the same rate. The match in fluid flow across the eight channels was very good, but not perfect; we observed the free surface of the fluid to oscillate up and down at a rate of about 1 mm/hour, with a total amplitude of 4 mm. The oscillations arise from the tendency of the system to self-correct for errors in the fluid level; if the level in the tank is too low, one of the suction hoses loses contact with the surface, and the fluid level increases until contact is regained. If the level is too high, the hydrostatic head of the system increases, retarding the incoming flow and augmenting the outgoing.

The placement of the four volume sinks at the surface of the tank perhaps deserves some comment. There are two issues here: the *motivation* for placing the sinks at the surface, and whether or not the sinks have any effect on the experiment. The motivation for placing the volume sinks at the surface rather than elsewhere arises from the overall objective of modeling the Earth's thermohaline circulation. There are, in fact, small volume fluxes involved in the ocean's circulation, in the form of precipitation and evaporation. As these fluxes occur exclusively at the ocean's surface, it is sensible to have all the volume fluxes in the laboratory experiment occur at the surface also.

However, the effect of the surface volume fluxes is small. This can be seen by comparing the surface volume flux V_s to the typical interior volume flux V_b generated by the buoyancy sources. If $V_s/V_b \ll 1$, then the volume flow through the surface is small compared to the volume circulating in the tank, and the surface volume flux plays a negligible part in determining the interior flow. Here, V_s = 0.15 ml/s; V_b can be estimated from Fig. 5 (and recalling that the tank is 4.5 cm thick) as being about 2 ml/sec. Thus, $V_s/V_b = 0.07 \ll 1$, and the surface volume flux makes little difference. As a matter of interest, this can be compared to the same ratio for the Earth's thermohaline circulation; the COADS data set (Woodruff et al., 1987) indicates an average value of net precipitation minus evaporation over the world ocean of about 1 mm/day, which is equal to 4 Sv. If we estimate the thermohaline circulation to involve about 30 Sv, then $V_s/V_b \approx$ 0.13 for the Earth, about twice as large as for the laboratory experiment, although still small; the volume flux effects in the laboratory experiment should therefore be correspondingly smaller than for the Earth.

Another method which might be used to estimate the importance of the surface volume flux would be to compare the average replacement time τ_r of a water parcel in the tank (which must be accomplished by the surface volume flux) to the average deep overturning time τ_o. If $\tau_o/\tau_r \ll 1$, then water circulates through the system many times before it is replaced, and so the replacement volume flux will have little influence on the flow pattern. With the tank volume of 6.6 $\times 10^{-3}$ m^3, $\tau_r = 4.4 \times 10^4$ sec; τ_o can be estimated from a typical interior velocity of .1 cm/sec and the tank length of .92 m to be about 2 $\times 10^3$ sec. Thus, $\tau_o/\tau_r = .04 \ll 1$. This again can be compared to the value for the Earth; assuming a typical overturning time of 500 years (Stuvier et al., 1983) and a surface exchange rate of 4 Sv yields $\tau_o/\tau_r \sim 0.5$, rather larger than the laboratory value.

b. Measurement Systems

Density measurements were made with a custom-constructed 4-wire density probe which used an actively-driven ("sucking") design. Fluid was pumped via a single-channel peristaltic pump into a micro-pipette 3 mm wide which housed the two sensing wires. The flow speed was typically .1 ml/sec; this constant flushing of the sensing wires ensured accurate readings without any problems due to stagnant boundary layers forming around the sensing wires. A drip chamber in the tubing ensured that the sensing volume was electrically isolated from the rest of the pumping system.

The probe was removed from the tank between samples to minimize the amount of fluid withdrawn from the tank by the probe's suction, dipped in a fresh water bath to wash the salt off, then air-dried. We found that without the rinse, inaccurate results could be generated by salt crystals, formed by evaporation of the saline test fluid, flaking off the probe housing and getting into the sample volume. Samples were typically taken every 5 minutes early in the experiment, and every 20 minutes later.

The probe was driven by custom electronics, and the generated output voltage (indicating conductivity) was sampled by a 16-bit analog to digital converter driven by a microcomputer. The UNESCO [1981] routines were used to generate salinities from the measured temperature and conductivity ratio.

The primary inaccuracy in the salinity measurements arises from calibration errors. The probe was calibrated by measuring the output voltage in solutions of known salinity, then fitting the conductivity ratio versus 1/voltage relationship to a straight line. The salinity solutions were made by dissolving a known weight of pure NaCl in a known weight of distilled water. The salinity of the calibration solutions is estimated to be accurate to about 2 percent.

All the horizontal velocity fields shown here, including both the instantaneous traces and the interior maximums, were measured by timing streaks of permanganate dye released from single permanganate crystals dropped into the tank. This leaves a vertical streak of dye which is subsequently advected by the flow field. The permanganate crystals were ground before being dropped to make them smaller and rounder. The procedure was recorded on videotape for analysis; the initial and final streak shapes were digitized from television monitors displaying freeze-frame images of the tapes. The primary source of error in the process is determining the position of the dye streaks, which are somewhat blurred after being advected. A typical uncertainty in the position of the dye streak of 0.2 cm after a total movement of 4 cm, which yields an estimate of the velocity errors of 5%. The uncertainties in the elapsed time are less than 1/30 of a second, with the timings supplied by the VCR, and are small by comparison.

The permanganate crystals were dropped 69 cm from the left hand edge of the tank, and centered between the front and back walls. This location was chosen because it was not strongly influenced by either the dense, descending plume to the right, nor the end wall to the left; in this region the flow was primarily horizontal and smooth, especially after the first 50 minutes or so of the experiment. When the topographic slope was used, it extended from the right hand edge leftwards for 18 cm.

The streak photograph was taken by seeding reflective particles into the flow field, then illuminating the tank with a thin sheet of laser light centered between the front and back walls. To keep the particles wetted, a thick, fresh surface layer was allowed to build up before the photograph was taken; this helped prevent the particles from floating on the surface. The scale along the top is in centimeters; the dense sources are located at X=84 and 86 cm, while the suction hoses can be seen at X=54 and 69 cm. The vertical projections coming a short way up from the bottom near X=60 and X=87 cm are screws while help hold the tank together. Note the slight keystoning of the picture.

3. Results

a. Control Case

Figure 2 shows contours of salinity as a function of depth and time for the control run, with no rotation and no bottom topography. A thin, fresh layer can be seen at the surface of the tank, formed by fluid from the light density source which has propagated across the surface of the tank. A sharp halocline has formed just beneath this layer. Using an approximate Rayleigh number of $\sim 1 \times 10^{14}$ (based on a value of

$\Delta S \approx 2\%$), the scalings of Rossby [1965] yields an estimate for the surface layer thickness of ≈ 1.3 mm, as opposed to the observed value, from Figure 2, of about 3 mm. The discrepancy likely has to do with the fact that the forcing is accomplished in this experiment by pumping in fresh water, which can accumulate on the surface, rather than a true, no-volume buoyancy flux.

The interior of the tank is well mixed, with only a slight vertical salinity gradient. The fluid in this volume recirculates rapidly through the driving plume, resulting in a large degree of mixing. Figure 3 shows a streak photograph of particle tracks in the control experiment, with an exposure time of 15 seconds. The right 0.45 m of the tank is shown. The chaotic sinking region can clearly be seen, along with the more laminar deep recirculation region. The distinct boundary between the surface freshwater layer and the deep, homogenous layer is also visible.

The average salinity as a function of time in the tank is shown in Fig. 4. It increases from the initial value of about 5.2% to 6.3% by the end of the run. This is due to a "short circuit" of the fluid flow into the tank. By this it is meant that the suction hoses along the top of the tank preferentially withdraw fresh water, since the fresh water tends to float along the surface. By definition, in steady state the average salinity pumped out of the tank must equal the average salinity of the fluid pumped into the tank. But this does not mean that the fresh and dense waters have to participate equally in the meridional circulation. For example, consider a degenerate situation where one of the two fresh sources feeds directly into one of the sinks, and does not participate in the circulation. It is still perfectly possible to reach a steady state; with a dense source of 10% salinity, the average salinity of the fluid pumped out of the three suction hoses not involved in the "short circuit" will be 6.6%, and, by assumption, the suction hose in the short circuit will withdraw fluid of 0% salinity. Fresh water is circulating through the system rapidly, with a short residence time in the tank in comparison to the dense water. If we assume that the remaining fresh water source and the two dense water sources contribute equally to the deep water, then the average residence time for the dense water is twice that of the fresh water. Oceanic waters have a similar behavior; since both evaporation and precipitation interact with the surface of the ocean only, the most recently precipitated water is the most likely to be evaporated.

The magnitude of this secular increase in salinity is small compared to the applied buoyancy dipole forcing. From Fig. 4, we see that the average salinity increases about 0.3 ppt in an hour, which is equivalent to a buoyancy flux of about 3.6 $\times 10^{-9}$ m^4 s^{-3}. This is close to an order of magnitude smaller than the buoyancy flux applied by the forcing dipole, 2.6×10^{-8} m^4/sec^3, and so has little effect on the flow field.

A representative single (unaveraged) trace of the horizontal velocity as a function of depth is shown in Fig. 5. This trace was taken in the center of the tank, about 23 cm from the right hand edge, by the permanganate dye methodology described in section 2b. The circulation is smooth and fairly symmetric about the horizontal zero-crossing line. Thus, much of the interior fluid never upwells through the halocline, but instead recirculates at intermediate and deep levels in the tank. All the horizontal velocity traces were digitized at the same levels, indicated by the dots on the figure; these will be omitted from future traces.

The time evolution of the interior velocity is shown in Figure 6. The quantity shown is the maximum of the deep horizontal velocity field, as measured by the dye streaks described in Section 2b. (The error bars represent estimated errors in the measured velocities, which arise primarily from uncertainties in estimating the position of the dye streak, and do not indicate measured variance of the velocities.) The velocity starts out relatively high, reaches an intermediate-time minimum after about 50 minutes (accompanied by noticeable variability in the measured velocities) then slowly increases.

This behavior is a result of the interaction of the light source with the dense source, and so is a unique characteristic of dipole-forced systems. When the experiment is first started, no information from the light source has yet reached the dense plume, so the velocities evolve as if the dense source alone were present. Using the plume equations given in Turner [1973], the expected horizontal velocity in this case can be calculated:

$$\mathrm{u_{max}} \approx 4\pi \frac{6}{5} \alpha^{4/3} \mathrm{z_E}^{5/3} (\frac{9}{10} F)^{1/3} \tag{1}$$

where $\mathrm{u_{max}}$is the maximum horizontal velocity flowing out of the plume's detrainment region, α is the entrainment constant (taken to be .1 for the control case), $\mathrm{z_E}$is the depth over which entrainment into the dense plume occurs, and F is the surface buoyancy flux. In calculating this, we have simply assumed that the velocity profile of the fluid flowing away from the detrainment region is roughly parabolic in both the vertical and horizontal directions, so that the volume flux out of the plume is approximately $\mathrm{u_{max}} A/4$, where A is the cross sectional area of the outflow.

Thus we see that the maximum horizontal outflow velocity is proportional to the buoyancy flux driving the system. As time progresses from T=0 to T=50 minutes, we see from Figure 6 that this velocity rapidly decreases. During this time buoyant fluid is accumulating on the surface of the tank, mixing with the dense descending fluid, and decreasing the effective buoyancy flux.

The degree to which buoyancy is accumulating in the top layer can be estimated directly from the density profile measurements. Let an "excess buoyancy" parameter S be defined as

$$S = \int_L^0 g\beta(s(z) - s_o)dz \qquad (2)$$

where L is chosen to be in the relatively homogeneous interior of the tank, $s(z)$ is the salinity at depth z and s_o is the salinity at depth L, β is the coefficient of haline contraction, and g is the gravitational constant. Thus S is a measure of the total accumulation of buoyancy in the surface layer, relative to the interior of the tank.

Figure 7 shows the evolution of S with time for the control run. There is initially no excess buoyancy, as the tank starts out in a well-mixed state. Between T=0 and T=50 minutes, there is a rapid accumulation of buoyancy in the surface layer, decreasing the effective buoyancy flux into the interior of the tank and steadily reducing the interior velocities. After about 50 minutes the excess buoyancy starts decreasing, and there is some indication in Figure 6 that the velocities increase gradually at the same time. This is coming about because salt is slowly diffusing across the sharp halocline, densifying the top layer, and increasing the buoyancy flux to the interior of the tank.

Figure 8 shows the correlation between the excess buoyancy parameter S from Fig. 7 and the maximum horizontal velocity from Fig. 6. As can be seen, there is generally a reasonable negative correlation between the two, with the exception of one outlier which has a low observed velocity for the measured buoyancy excess parameter. This point occurred early in the experiment (T=30 min) and the low velocity is likely related to eddy activity which was observed in the tank at the early times, but died off after about 50 minutes.

b. The Effect of Bottom Topography

To force a change in the entrainment profile underneath the dense source, we inserted a sloping bottom into the tank, at approximately a $45°$ angle. The extent to which this would be expected to decrease the entrainment can be judged as described by Turner [1973]; the slope Richardson number $\mathrm{R_i} = g'h\cos\theta/U^2$ is about 1, where g' is the reduced gravity, h is the thickness of the downward-flowing layer (≈ 1 mm), θ is the angle of the slope, and U is the mean along-slope velocity (≈ 1 cm/sec). Figure 6.8 of Turner [1973] shows that for this slope Richardson number the entrainment parameter, α, should be about .001. By contrast, $\alpha \approx .1$ for the control run; thus, the presence of the slope inhibits entrainment by a substantial amount.

The evolution of the horizontal velocity maximum for the bottom topography case is shown in Figure 6. The initial velocity is similar to that of the control case, but rapidly drops to a lower value and remains there. Additionally, there is no evidence of a slow increase in velocity after the first minimum, as can be seen in the control case.

An important difference between the control case and the case with bottom topography is in how the horizontal velocity as a function depth changes over time. In the control case, the *amplitude* of the velocity versus depth curve evolves over time, as shown in Fig. 6. However, the vertical *pattern* is always the same; it is always about sinusoidal, with leftward and rightward branches of approximately equal thickness, as shown in Fig. 5. By contrast, in the case with bottom topography, the horizontal velocity as a function of depth after a long time looked very unlike its initial profile, as will now be described.

When the experiment was first turned on, the dense fluid flowed to the bottom of the slope, and entered the interior in a thin horizontal ribbon along the bottom. As time went on, the depth at which this flow detached from the slope and flowed into the interior rose higher and higher into the water column, so that after three hours it was relatively near the halocline. Thus the laboratory model's equivalent of "deep" water evolves over time to become an "intermediate" water mass. Horizontal velocity profiles as a function of depth and time, illustrating this behavior, are shown in Figure 9.

It seems evident that this evolution is due to the pronounced bottom density maximum pushing the neutral level for the descending plume ever higher into the water column. However, there are subtleties involved, since the presence of the dipolar forcing is critical to observing this effect; in the monopolar-forced case there is a similar bottom density maximum, and yet the plume always penetrates to the bottom (Baines and Turner, 1969). This effect then arises exclusively from the interaction of the presence of a dipolar source and bottom topography. An analysis of this interaction will be presented in Section 5.

Figure 10 shows contours of salinity as a function of depth and time for the case with a bottom slope present under the dense source. The density shows a much more pronounced bottom density maximum, compared to the case without the slope. The tank is essentially filling from the bottom up, since (at early times) the dense water can reach the base of the slope with very little entrainment. Thus, the presence of the bottom topography greatly influences the tank's density structure on the early to intermediate time scales.

Also shown in Fig. 10 are the approximate upper (triangles) and lower (squares) limits of the region over which the heavy plume detrains. These limits were identified from horizontal velocity traces such as shown in Figure 9. The lower limit was taken to be the depth of the first local velocity minimum deeper then the global velocity maximum, or the bottom, if there was no such minimum. As can be seen from Fig. 9, most traces had a well defined local minima of this type. The upper limit of the detrainment region was taken to be the depth of the first local minimum *above* the global maximum, or the depth of the velocity zero-crossing, whichever was deeper; for each of the five traces of Figure 9, this upper limit is shown by a heavy black dot. It can be seen that for most traces, the location of the zero-crossing determines the upper boundary of the region.

c. The Effect of Rotation

Baines and Turner [1969] performed a laboratory experiment examining the fashion in which a monopolar density source builds a pycnocline in a confined region. We performed essentially an identical experiment in a rotating environment, to determine the influence of rotation on the evolved density structure.

For this experiment only, a cylindrical tank was used, to correspond more closely to Baines and Turner

[1969]. The tank was 30 cm in diameter, and filled with a distilled water/salt solution to a height of 20 cm. The initial salinity was set to be about 15 ppt, which is the minimum salinity the density probe can resolve; in this fashion, all salinity changes could be measured. A tube in the center of the tank supplied a saturated salt solution (23% salinity) at a rate of .2 ml/sec, which at a salinity difference of 21% is a buoyancy flux of 2.9×10^{-7} m^4/sec^3. The rotation rate was 1.2 radians/second.

Vertical salinity profiles were taken continuously, at a high plunge speed for the probe (about 1 cm/sec). Additionally, the probe was scanned horizontally in the tank between traces, sampling at one of 11 predetermined sites. This was done so that horizontal variations in the tank could be determined, and averaged out if desired.

Figure 11 shows vertical salinity profiles for the non-rotating (control) and rotating cases. The traces shown are horizontally averaged across the 11 stations in the tank, and temporally averaged between 45 and 75 minutes. The traces are offset so that the deepest salinity value of each is zero, so the two can be compared more easily. The traces actually differed by 2.5 ppt at the deepest level, probably due to a minor difference in the initial, probe bias salinity. As can be seen from the figure, there is very little difference between the rotating and non-rotating cases. The rotating case is perhaps a bit better mixed in the deep part of the tank, but the difference small at best.

An additional aspect of the difference between the rotating and non-rotating cases can be seen in Figure 12, which shows the r.m.s. variance in the measured salinity as a function of position within the tank. The non-rotating case shows most of the variance concentrated in the center of the tank, near the location of the dense plume. The rotating case, on the other hand, has the variance spread more evenly over the tank. Observations of the tank-filling process showed that in the rotating experiments, a dense column of fluid formed under the source and subsequently broke away from the source and propagated into the center of the tank. This is similar to the behavior observed by Helfrich and Battisti [1991] in an initially stratified (rather than initially homogeneous, as used here) environment.

This experiment suggested, then, that the *manner* in which the tank filled was significantly more affected by the presence of rotation than was the ultimate vertical density distribution. It should be kept in mind that the diameter of the tank (30 cm) was only about 30 times the observed diameter of the vortices ($\sim$ 1 cm), and the propagation velocities of the vortices was fairly substantial ($\sim$ 1 cm/sec), so that the walls of the tank were encountered early in the lifetimes of the vortices; this may have an overriding influence on this observation.

The convection in a slot experiment was also performed with a rotation rate of 1 radian/sec. Contours of salinity as a function of time and depth for the rotating run are shown in Figure 13. There are a number of apparent differences between the rotating case and the control (Figure 2). The primary difference is that the surface halocline seems to be spread over a much greater depth; in the control run it is about 3 mm, but in the rotating case it seems to be generally spread out over the top 2 cm. This implies an enhanced mixing mechanism, likely associated with the vortices which form under the sources and sinks. Visual observations showed a persistent eddy centered under the dense source, which occasionally broke away and propagated into the interior of the tank. The origin of the features seen in Figure 13 at .25, 1.1, and

1.9 hours are likely just such events. No comparable events were seen in either the control or bottom slope test cases. Lastly, it can also be seen in the figure that the overall noise level is higher, reflecting the fact that the density probe is in an electrically noisier environment, and has had its output passed through the slip rings.

4. Analysis

The system can be thought of as evolving on three distinct time scales: an advective time scale, a short diffusive time scale, and a long diffusive time scale.

a. Advective Time Scale

When the experiment is first switched on, the experiment evolves rapidly through advective processes. Fluid modified by the light source propagates rapidly across the surface of the tank in a gravity current, setting up a strong, top-trapped circulation. Fluid from the dense source convects into the interior, spreads out at a neutral level (or, barring that, at the bottom), and fills the tank. Although the light surface evolution is not modified appreciably by the presence of bottom topography, the same cannot be said for the deep evolution. The time which it takes the interior of the tank to participate advectively is set by the volume of the tank divided by the net volume flux from the dense source. Since the net volume flux from the dense source is a strong function of the entrainment rate, this time will be substantially longer in the case where bottom topography is inhibiting entrainment. This is suggested by Figure 6, which shows the time evolution of the maximum horizontal velocity in the case with bottom topography (along with the control case for reference). It can be seen that the velocities are almost a factor of 10 lower when bottom topography is present. If we simply assume that the detrainment region is about the same thickness in the two cases, then the advective time scale to set up the circulation in the interior of the tank will be about 10 times longer when topography is present. In actuality it will be longer still, since the detrainment region is thinner when topography is present.

b. Short Diffusive Time Scale

The laboratory system approaches the ideal of being forced with a pure buoyancy flux, but actually has a small volume flux associated with the forcing in addition. The light, incoming fluid forms a thin, fresh skin on top of the tank, and must come to diffusive equilibrium with the underlying fluid. It is this densification of the surface layer which is responsible for the slow increase in surface salinity. This increases the interior velocity starting after 50 minutes, which can be seen in Figure 6.

The time scale over which diffusion into the surface layer should become important can be estimated as $\tau \sim l^2/\kappa$, where l is the thickness of the surface layer and κ is the diffusion constant for salt. Using l = 3 mm and taking $\kappa = .7 \times 10^{-9}$ m^2/s yields $\tau \approx 45$ minutes, in reasonable agreement with the time scales seen in Figure 7.

In some situations shear instabilities across the sharp pycnocline might contribute to the mixing. This tendency can be described in terms of a Richardson number $\mathrm{R_i} = gh\Delta\rho/[\rho_o(\Delta u)^2]$, where g is the gravitational acceleration, and h is the thickness of an interface with density jump $\Delta\rho$ and velocity jump Δu. For the experiments shown here $\mathrm{R_i} \gg 1$, and shear instabilities should not be important.

c. Long Diffusive Time Scale

It was observed that the cases with bottom topography tended toward a state where all the circulation was top-trapped, with little ventilation of the deep waters. It is interesting to conjecture whether this is a possible long-term equilibrium solution of the system. By hypothesis, in such a case there would be no vertical advective salt transports. However, the continuing existence of a vertical salinity gradient would still generate diffusive transports, which would slowly freshen the deep water. The plume would then have a tendency to sink to the bottom of the tank again, re-ventilating the deep water. The top-trapped circulation therefore cannot be an equilibrium solution.

It is also interesting to note that only in the case with bottom topography was the "lifting" of the dense plume off the bottom of the tank observed. As the bottom topography case suppresses entrainment, leading to a more pronounced bottom density maximum, this behavior seems at least qualitatively reasonable. It is examined more quantitatively with a simple "plume" model developed in the next section.

5. A Simple Plume Model

The evolution of the system over times long compared to the diffusive timescale of the entire tank is not easily examined in the laboratory. Using salt and a characteristic depth of .16 m, an estimate of the diffusive timescale can be given by $\tau \sim l^2/\kappa \sim 1$ year, too long to examine in the lab. However, the behavior can be examined more closely with a simple numerical model of the behavior of a plume in a stratified tank. The philosophy of the model is straightforward: given a background stratification, plume conservation equations can be integrated to yield the behavior of a turbulent plume in that environment; and given the vertical structure of a turbulent plume, the plume's influence on a background stratification can be determined. Thus by alternately solving for the structure of the plume and the environment, the system can be stepped forward in time.

The basic plume equations are derived in a manner similar to Morton et al. [1956]. The conservation of volume, momentum, and density deficiency can be expressed as

$$\begin{aligned}
\frac{d}{dz}\left(b^2 u\right) &= 2\alpha(z) b u \\
\frac{d}{dz}\left(b^2 u^2\right) &= \frac{b^2 g}{\rho_o}\left(\Delta_1 - \Delta_2\right) \\
\frac{d}{dz}\left(b^2 u \Delta_1\right) &= 2 b \alpha(z) u \Delta_2
\end{aligned} \tag{3}$$

where b is the radius of the dense plume, u is the vertical velocity, $\alpha(z)$ is the entrainment ratio (now a function of depth), g is the acceleration due to gravity, $\Delta_1 = \rho_o - \rho_{plume}$, $\Delta_2 = \rho_o - \rho_{environ}$, and ρ_o is the environmental density at the top of the tank. A linear equation of state is used.

Defining the auxiliary variables

$$\begin{aligned}
m &= b^2 u \\
v &= b u
\end{aligned} \tag{4}$$

$$f = m\Delta_1$$

the set of equations 3 can be rewritten as

$$\begin{aligned}
\frac{dm}{dx} &= 2\alpha(z)v \\
\frac{dv^4}{dx} &= \frac{2g}{\rho_o} m\,(f - m\Delta_2) \\
\frac{df}{dx} &= 2\alpha(z)v\Delta_2
\end{aligned} \tag{5}$$

Here, m is the vertical mass flux, v^2 is the vertical momentum flux, and f is the vertical buoyancy flux, taken relative to the top of the tank. Boundary conditions are $m = v = 0$ and $f = \rho_o B_o / g\pi$ at the top surface, where B_o is the buoyancy flux driving the plume.

We add to this a vertical conservation equation for an environmental tracer T, here taken to be heat:

$$\frac{\partial T}{\partial t} = w_e \frac{\partial T}{\partial z} + \kappa \frac{\partial^2 T}{\partial z^2} \tag{6}$$

where κ is the appropriate diffusion constant. Heating of Q Watts is applied as a constant flux condition at the upper surface, such that the positive buoyancy flux into the system from the heating equals the negative buoyancy flux driving the plume: $Q = B_o \rho_o c_p / g\beta$, where β is the thermal expansion coefficient. Thus the system has a dipolar type of forcing, with a concentrated cold point producing the plume, and diffuse heating warming the rest of the surface.

The vertical velocity in the tank, w_e, is calculated from the conservation of mass requirement that $F_p + F_i = F_o$, where the fluxes F are as shown in Figure 14, along with the requirement that there are no mass fluxes through the top or bottom.

In the results shown here, the set of Equations 5 and 6 are solved using a Runge-Kutta scheme on the grid shown schematically in Figure 14. The grid which the plume equations were solved on is determined by consideration of the errors involved due to the grid spacing at the previous timelevel (Press et al., 1989), and changes every iteration to increase coverage in regions of large background vertical gradient. Values are then remapped onto the regular grid which describes the background environment of the tank. To preserve high accuracy in the plume equations, there are typically a hundred times as many gridlevels in the plume as there are in the environment.

Derivatives of v are singular at $x = 0$, which complicates the solution procedure; to get around this, the solutions are initialized with algebraic expansions valid about $x = 0$, as described in Morton et al. [1956].

Because the plume equations do not include the detrainment physics, a parameterization for this mechanism needs to be applied. The detrainment used here is based on the depth at which the plume becomes neutrally buoyant, h_0, and at which the vertical velocity goes to zero, h_1. In general h_1 is deeper than h_0 (i.e., the plume overshoots the depth of neutral buoyancy) because there is excess momentum at the neutral depth, which carries the plume farther; the plume then falls back and detrains somewhere between these heights (Turner, 1973). To simulate detrainment, the following principles are applied in the detrainment region: 1) heat is conserved, so that heat fluxed into the detrainment region from the plume must eventually flow from the detrainment region to the environment; 2) The detrainment should vary smoothly between zero at the top and bottom of the detrainment region, and reach a maximum in between.

The form of this function is simply taken to be an error function:

$$\mathcal{V}(z) = \pi b^2 u \left(1 - \mathrm{erf}\left(\left(z - h_{\frac{1}{2}}\right)/z_l\right)\right) \tag{7}$$

where $\mathcal{V}$ is the vertical volume flux in the plume, $h_{\frac{1}{2}}$ is a point halfway between h_0 and h_1, and z_l is a detrainment length scale, here taken to be $(h_0 - h_1)/3$. The volume flux out of the plume is then simply $d\mathcal{V}/dz$. Applying a weighting function in the detrainment region is necessary because although the vertical velocity of the plume is going to zero at the bottom of the detrainment region, the radius of the plume is spreading towards infinity; the result is that $\mathcal{V}$ approaches a constant value. Thus, if the plume is presumed to detrain somewhere, the vertical volume flux has to be brought to zero. Applying the weighting function on $\mathcal{V}$ is particularly appealing because the formulation automatically conserves mass; the volume flux into the detrainment region must necessarily equal the volume flux out.

If h_0 or h_1 is greater than the depth of the tank, then they are set equal to that depth; and if the thickness of the detrainment region, $h_0 - h_1$, is less than $.85b$, then it is set equal to that value. The value .85 is chosen because it is the diameter of the largest circular eddy which can be inscribed in the descending plume's cone.

It is important to note that this simple model is calculated as a succession of quasi-steady states, rather than using truly time-dependent versions of Equations 3. However, the system is fully coupled; the plume builds the stratification in the tank, and the stratification acts back on the plume, affecting the depth at which the plume detrains. The quasi-steady state assumption is equivalent to saying that the processes which determine the form of the plume occur on a much shorter time scale then the processes which determine the background stratification in the tank. This is true as long as the volume flux out of the plume fills the tank slowly compared to a plume timescale:

$$\frac{\mathcal{V}_p \tau_p}{V_t} \ll 1 \tag{8}$$

where $\mathcal{V}_p$ is the volume flux out of the plume, τ_p is a characteristic plume time scale (which may be taken as the time a parcel takes to vertically traverse the plume); and V_t is the volume of the tank. In the laboratory experiments described above, $\mathcal{V}_p \sim 2 \times 10^{-5}$ m^3/sec, $\tau_p \sim 6$ sec, and $V_t \sim 8 \times 10^{-3}$ m^3, yielding a ratio of about .015.

Contours of density as a function of time and depth for the plume model control run are shown in Figure 15. The model evolution can be directly compared to Figure 2. The correspondence is quite good; in both cases there evolves a thin, light surface layer, along with a deep, well-mixed layer. The vertical volume flux $\mathcal{V}$ in the model plume is shown as a function of depth at T=30, 60, and 180 minutes in Figure 16. Since mass in the tank is conserved, this is also the vertical volume flux in the tank environment outside of the plume. Since the volume of the tank environment is not varying appreciably with depth (unlike the plume's volume), $\mathcal{V}$ is directly proportional to the vertical velocity in the tank, while the horizontal velocities in the tank are proportional to $d\mathcal{V}/dz$. As can be seen from the figure, the majority of fluid recirculates deep in the tank, with little exchange through the surface pycnocline. As the experiment progresses, the plume must penetrate into an increasingly stratified environment; the deep volume flux consequently decreases with time, and the plume detrains higher in the water column.

To compare the model results to the laboratory system with the bottom slope inserted under the dense source, the entrainment parameter was allowed to vary in depth as shown in Figure 17. It drops in a smoothed-step fashion from a surface value of 0.1 to a deep value of 0.001. The deep value was taken to correspond to the calculated laboratory value, as described in Section .

Figure 18 shows contours of temperature as a function of depth and time for the plume model case with the depth-varying entrainment parameter. This figure can be directly compared to Figure 10, the laboratory result. Again, the correspondence is quite good.

As can be seen in Figure 18, the plume "lifts off" the bottom of the tank, detraining at successively shallower depths, and then slowly settles back to the bottom of the tank. The origin of the "lifting off" behavior is illustrated schematically in Figure 19. Consider a plume of dense fluid which enters a homogeneous body of water and detrains on the bottom of the tank. Initially, the density in the environment will be lighter than the fluid injected by the plume; consequently, the average density of the water in the slab of fluid being fed by the plume will increase with time. If the system is forced by a source/sink dipole, then a steady state can be reached; in steady state, the density of fluid in the slab being fed by the plume will become the same as the density of the plume. If the density of the plume suddenly decreases after this equilibrium is reached, the plume will be too light to penetrate through to the bottom, and so will lift off the bottom of the tank (neglecting, for simplicity, the tendency of plumes to overshoot their neutral level). If the change in density of the plume occurs before equilibrium has been reached, then the behavior depends on the magnitude of the change: if the new density of the plume is less than the instantaneous density of the environment, the plume will lift off. Otherwise, it will simply continue to densify the bottom.

The lifting off behavior can thus be seen as a competition with contributions from two effects: a) the time at which the plume changes density, compared to the time which the environment takes to equilibrate with the plume. In the limit that the environment is completely equilibrated with the plume, then (neglecting the overshoot effect) a decrease in plume density will always cause lifting off. b) the magnitude of the change in plume density, compared to the initial density difference between the plume and the environment. In the limit as the decrease in plume density exceeds the original density difference between the plume and the environment, the plume will always lift off.

This can be summed up by considering the ratio

$$\frac{\Delta\rho\Delta t\mathcal{V}_p}{\Delta\rho_o V_o} \tag{9}$$

where $\Delta\rho$ is the change which the plume density undergoes, Δt is the time at which the plume change occurs, $\mathcal{V}_p$ is the volume flux from the plume which feeds an environment of volume V_o, and $\Delta\rho_o$ is the difference in density between the plume and environment at time T=0.

6. Comparison to Oceanic Observations

As discussed in the introduction, the physical system of interest here is the Earth's thermohaline circulation. Although an insufficient time series of observations exists to adaquately document the time evolution of the large scale thermohaline circulation, there are nontheless some observations which can be used over shorter time spans or as instantaneous snapshots of the processes involved. These can be generally broken into two groups: open ocean convective sites (exemplified by the Labrador Sea), and convective sinking along continental margins, as exemplified by the Mediterranean outflow (see also the discussion in Killworth [1983]). The open ocean convection sites are analogous to the laboratory "control" experiments, while the regions of sinking along margins is like the topographic slope test case.

Observations of convectively-formed Labrador Sea Water (LSW) are presented in Clarke and Gascard [1983]. These are interesting becuase they show a distinct time evolution of the properties of LSW, which chilled by 0.5 C and freshened by 0.05 ppt between 1966 and 1976. Moreover, the Great Salinity Anomaly (GSA) (Dickson et al., 1988) shut off convection in the Labrador in the mid 1980s (Lazier, 1988), but later observations show that convection has resumed in the 1990s (J. R. N. Lazier, *personal communication*). The shutoff of convection in response to the light surface cap of the GSA advected into the region is reminescent of the laboratory model's behavior soon after turnon, when the fresh water from the lightening source propagates across the surface and reaches the dense source. The laboratory model does not completely cease convecting in response, but the rate of overturning does drop sharply, as can be seen in Fig. 6.

One interesting difference between the LSW observations and the laboratory experiment is that the *density* of the LSW remained relatively constant during these temperature and salinity variations; the cooling and freshening occured in approximately the correct ratio to accomplish this. The laboratory experiment, by contrast, has only one active density component (salinity), so no such compensation is possible. Therefore, the "lifting off" of the dense bottom plume in the topographic slope test case, which is due to lightening of the source by freshening, might be less likely to occur in nature were the source waters to compensate for the freshening by becoming colder. On the other hand, the T, S compensation which has kept LSW at an approximately constant density seems to have been overcome in the last two years, as the depth of convection has reached the top of the underlying, salty, NADW (J. R. N. Lazier, *personal communication*).

The Mediterranean Sea outflow is interesting in that it is similar to "arrested" form of the bottom plume lift-off which the topographic slope test case undergoes: the dense Mediterranean water flows down the continental margin, entraining along the way, but reaches a neutral density level and leaves the slope at mid-depth (Price et al., 1993). The outflow velocity is, then, reminescent of the later time traces in Fig. 9. The time evolution of the Mediterranean and the laboratory system are naturally quite different; in the laboratory case, the plume's lift off the bottom occurs because of time-varying properties of the dense plume, while the Mediterranean Sea overflow does not reach the bottom because of strong entrainment of lighter surface waters (Price et al., 1994). Interestingly, it has been suggested that the bottom waters of 50 million years ago were much warmer (15 C), and hence originated in low-latitude evaporation basins such as the Mediterranean (Brass et al., 1982). Such changes are driven by geological activity (i.e., changes in the shape of the ocean basins) rather than internal processes, which cause the time-dependent behavior of the laboratory experiment, but the end effect on the sinking plumes is probably similar.

7. Conclusions

We have described a number of laboratory experiments and a simple "plume" model designed to examine the convective building of a pycnocline, and how that process is affected by the following mechanisms: 1) the use of a dipole of surface density forcing, rather than a simple monopole; 2) the effect of changing entrainment under the dense source; 3) the presence of rotation as the system comes to equilibrium.

Forcing by a dipole of buoyancy fluxes on the same geopotential surface results in a final density distribution significantly different from that obtained using either a monopolar source, or a dipole of forcing on opposite surfaces. In the monopolar case the system comes to one of two rather straightforward equilibrium solutions: either approaching the density of the source (for a fixed-value boundary condition) or lightening or densifying indefinitely (for fixed-flux boundary conditions). When unstable dipolar forcing is applied on opposing geopotential surfaces, overturning cells of various configurations result.

Forcing with a dipole on the same geopotential—the more large-scale, geophysically relevant configuration—produces a final situation distinctly different in character. In this case, horizontal velocities must evolve which carry buoyancy from the source to the sink in the fluid. In the laboratory experiments, a thin, light surface layer forms beneath a thick, well-mixed layer. A tank-scale overturning cell develops, driven by the dense source, and drives much of the deep interior mixing by recirculating fluid through the descending plume.

When a topographic slope is present underneath the dense source, the dense plume undergoes much less entrainment as it sinks through the water column; as a result, the plume reaches the bottom with a smaller volume flux but a larger density. It was observed in the laboratory experiments that this tended to fill the tank from the bottom up, producing a much larger bottom density maximum then the case without the bottom slope.

One consequence of this larger bottom density maximum was that the dense plume was observed to “lift off” the bottom of the tank. This occurred when the surface buoyancy from the fresh source began modifying, a finite time after the experiment was started, the density in the descending plume. As a result, the density of the plume decreased, and detrainment occurred at successively shallower depths in the water column.

The ultimate stability of this situation was examined with a numerical “plume” model, which embedded the conservation equations for a dense plume sinking through a stratified environment with a tracer conservation equation for the background density field. The model showed that the plume must eventually lower back onto the bottom of the tank, because if the deep water is not being ventilated, diffusive transports will erase any vertical density gradients. This diffusion will continue until the plume once more descends to re-ventilate the deep water.

This process can be summarized as progressing on the following three time scales:

1) A short advective time scale. This is the time it takes the light water from the fresh source to propagate across the top of the tank, and begin interacting with the dense source. Until this happens, the

dipolar-forced experiment evolves similarly to the uniploar-forced case: a dense plume cascades to the bottom of the tank, and increases in density since it immediately starts re-entraining previously detrained water, which is heavier than the original background fluid. Once the light fluid reaches the dense source, this trend is reversed and mixing of the light and dense sources begins to lighten the fluid in the sinking plume.

2) A short diffusive time scale. This is the time over which diffusion acts to equilibrate the surface layer of water pumped in from the light source. This is an artifact of the departure of the laboratory system from the idealized case: in the laboratory, the buoyancy flux is accomplished with a small but finite volume flux, while in the idealization, the forcing is accomplished without any volume flux. Nevertheless, this results in an interesting mid-time minima in the velocities evolved by the laboratory system; after this time, diffusion salinifies the light surface layer enough to begin increasing the deep density flux somewhat.

3) A long diffusive time scale. This is the time over which the plume, which can rise off the bottom of the tank and detrain higher in the water column, will come back to detrain at the bottom again. The plume lifts off because the density of the plume decreases once the buoyant surface fluid starts getting entrained in the descending plume; the plume will only sink back to the bottom when the density which the plume injected at the bottom before this happened vertically diffuses away.

Rotation has an interesting effect on the manner in which the experiment comes to equilibrium. The quintessential case is expressed in the filling a confined region by a monopolar dense source, when the entire system is rotating. In this case, rotational constraints prevent the plume from simply sinking to the bottom and flowing outward; instead, columns of dense fluid form under the source, and eventually go baroclinically unstable and propagate into the interior of the fluid. The eventual filling of the box is accomplished when the baroclinic eddies spin-down due to dissipation. The mechanism by which the box is filled is thus vastly different when the system is rotating.

*List of References

Baines, W. D. and Turner, J. S. (1969). Turbulent buoyant convection from a source in a confined region . *J. Fluid Mech.*, 37:51–80.

Boubnov, B. M. and Golitsyn, G. S. (1990). Temperature and velocity field regimes of convective motions in a rotating plane fluid layer. *J. Fluid Mech.*, 219:215–239.

Brass, G. W., Southam, J. R., and Peterson, W. H. (1982). Warm saline bottom water in the ancient ocean . *Nature*, 296:620–623.

Chandrasekhar, S. (1953). The instability of a layer of fluid heated from below and subject to coriolis forces. *Proceedings of the Royal Society A*, 217:306–327.

Clarke, R. A. and Gascard, J. C. (1983). The Formation of Labrador Sea Water. Part I: Large-Scale Processes . *J. Phys. Oceanogr.*, 13:1764–1778.

Dickson, R. R., Meincke, J., Malmberg, S-A, and Lee, A. J. (1988). The 'Great Salinity Anomaly' in the Northern North Atlantic 1968-1982. *Progress in Oceanography*, 20:103–151.

Fernando, H. J. S., Boyer, D. L., and Chen, R. R. (1989). Turbulent thermal convection in rotating and stratified fluids . *Dynamics of Atmospheres and Oceans*, 13:95–121.

Fernando, H. J. S., Chen, R. R., and Boyer, D. L. (1991). Effects of rotation on convective turbulence . *J. Fluid Mech.*, 228:513–547.

Helfrich, K. R. and Battisti, T. M. (1991). Experiments on baroclinic vortex shedding from hydrothermal plumes . *J. Geophys. Res.*, 96:12511–12518.

Hignett, P., Ibbetson, A., and Killworth, P. D. (1981). On rotating thermal convection driven by non-uniform heating from below. *J. Fluid Mech.*, 109:161–187.

Hopfinger, E. J., Browand, F. K., and Gagne, Y. (1982). Turbulence and waves in a rotating tank . *J. Fluid Mech.*, 125:505–534.

Killworth, P. D. (1983). Deep Convection in the World Ocean . *Reviews of Geophysics and Space Physics*, 21:1–26.

Lazier, J. R. N. (1988). Temperature and salinity changes in the deep Labrador Sea, 1962-1986. . *Deep Sea Research*, 35:1247–1253.

Morton, B. R., Taylor, G., and Turner, J. S. (1956). Turbulent gravitational convection from maintained and instantaneous sources . *Proceedings of the Royal Society A*, 234:1–23.

Press, W. H., Flannery, B. P., Teukolsky, S. A., and Vetterling, W. T. (1989). Numerical Recipes . Technical report, Cambridge University Press.

Price, J. F., Baringer, M. O., Lueck, R. G., Johnson, G. C., Ambar, I., Parrilla, G., Cantos, A., Kennelly, M. A., and Sanford, T. B. (1993). Mediterranean outflow mixing and dynamics . *Science*, 259:1277–1282.

Price, J. F., O'Neil, and Baringer, M. (1994). Outflows and deep water production by marginal seas . *Progress in Oceanography*, 33:161–200.

Rossby, H. T. (1965). On thermal convection driven by non-uniform heating from below: an experimental study . *Deep Sea Research*, 12:9–16.

Stommel, H. (1962). On the smallness of sinking regions in the ocean . *Proceedings of the National Acadamy of Sciences, Washington*, 48:766–772.

Stuvier, M., Quay, P. D., and Ostlund, H. G. (1983). Abyssal water carbon-14 distribution and the age of the world oceans. *Science*, 219:849–51.

Turner, J. S. (1973). Buoyancy effects in fluids . Technical report, Cambridge University Press.

UNESCO (1981). Unesco technical paper in marine science number 36 . Technical report, UNESCO.

Woodruff, S. D., Slutz, R. J., Jenne, R. L., and Steurer, P. M. (1987). A comprehensive ocean-atmosphere dataset . *Bull. Amer. Meteor. Soc.*, 68:1239–1250.

Figure Captions

Fig. 1. Schematic of the laboratory setup for the experiments examining convection into a slot geometry.

Fig. 2. Contours of salinity as a function of depth and time for the control run, with no rotation or bottom topography. The upper one centimeter of the plot is on an expanded scale.

Fig. 3. A streak photograph of particle tracks in the control experiment. The exposure time was 15 seconds.

Fig. 4. Average salinity in the tank as a function of time, for the control case.

Fig. 5. The horizontal velocity as a function of depth, control case. This trace was taken after three hours; the pattern was unchanging after the first few minutes of the experiment.

Fig. 6. The time evolution of the maximum interior velocity for the control and bottom topography cases.

Fig. 7. The time evolution of the buoyancy excess parameter, S, for the control case.

Fig. 8. The excess buoyancy parameter S ($\mathrm{m}^2/\mathrm{sec}^4$) versus the maximum observed horizontal velocity.

Fig. 9. The time evolution of the horizontal velocity profile. Times shown are after initiation of the experiment. Negative velocities indicate flow away from the sinking plume.

Fig. 10. Contours of salinity as a function of depth and time for the case with sloping bottom topography. The dashed lines show the approximate upper (triangles) and lower (squares) boundaries of the detrainment region, as defined in the text. The top 1 centimeter of the plot is on an expanded scale.

Fig. 11. Vertical salinity traces taken while filling a confined region from a monopolar density source.

The traces are averaged, both across the tank width and in time. The rotating case has Ω = 1.2 radians/sec.

Fig. 12. R.M.S. variance in the measured values of salinity in the tank, for the control (top) and rotating (bottom) cases. For the rotating case, Ω = 1.2 radians/sec.

Fig. 13. Contours of salinity as a function of depth and time for the rotating case. Ω = 1.0 radians/sec.

Fig. 14. Schematic of the configuration of the numerical plume model. The actual grid has 50 layers in the environment, and a variable number in the plume.

Fig. 15. Contours of density (Kg/m^2) as a function of depth and time for the plume model control run with a constant entrainment parameter.

Fig. 16. The plume model's vertical volume flux (cubic meters per second) as a function of depth, for the control run with a constant entrainment parameter.

Fig. 17. The plume model's entrainment parameter, α, as a function of depth for the test case simulating bottom topography under the dense source.

Fig. 18. Contours of temperature (C) as a function of depth and time for the plume model with depth-varying entrainment. Crosses and triangles mark the top and bottom of the detrainment region, respectively.

Fig. 19 Schematic illustrating the origins of the "lifting off" behavior. The left hand panel shows the situation for small density changes in the plume; the right hand panel, for large density changes. Each of the two panels shows two cases: one for a change which happens in a time short compared to the plume/environment equilibration time (the solid lines), and one of which is for a time long compared to the equilibrium time (dashed lines).

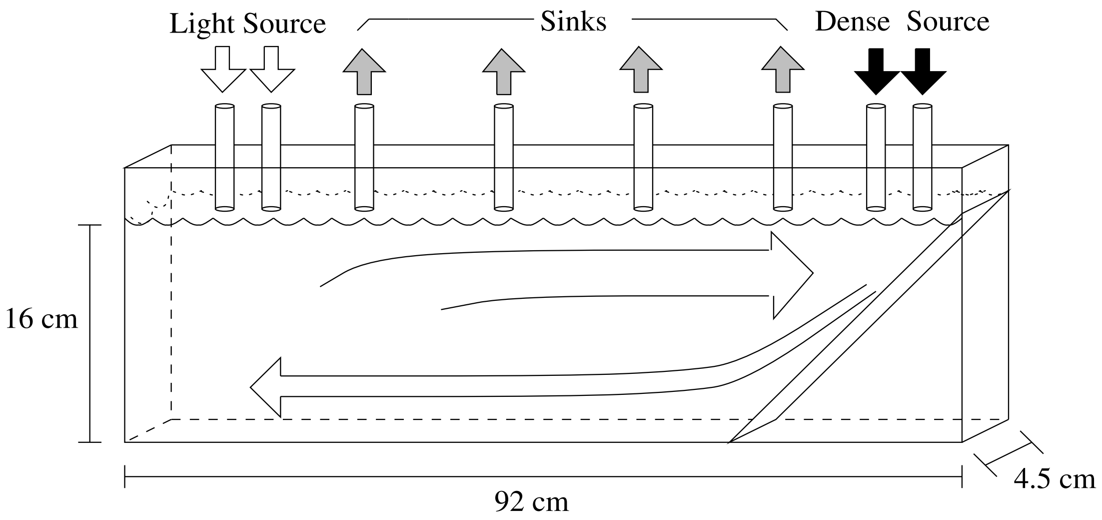

Figure 1:

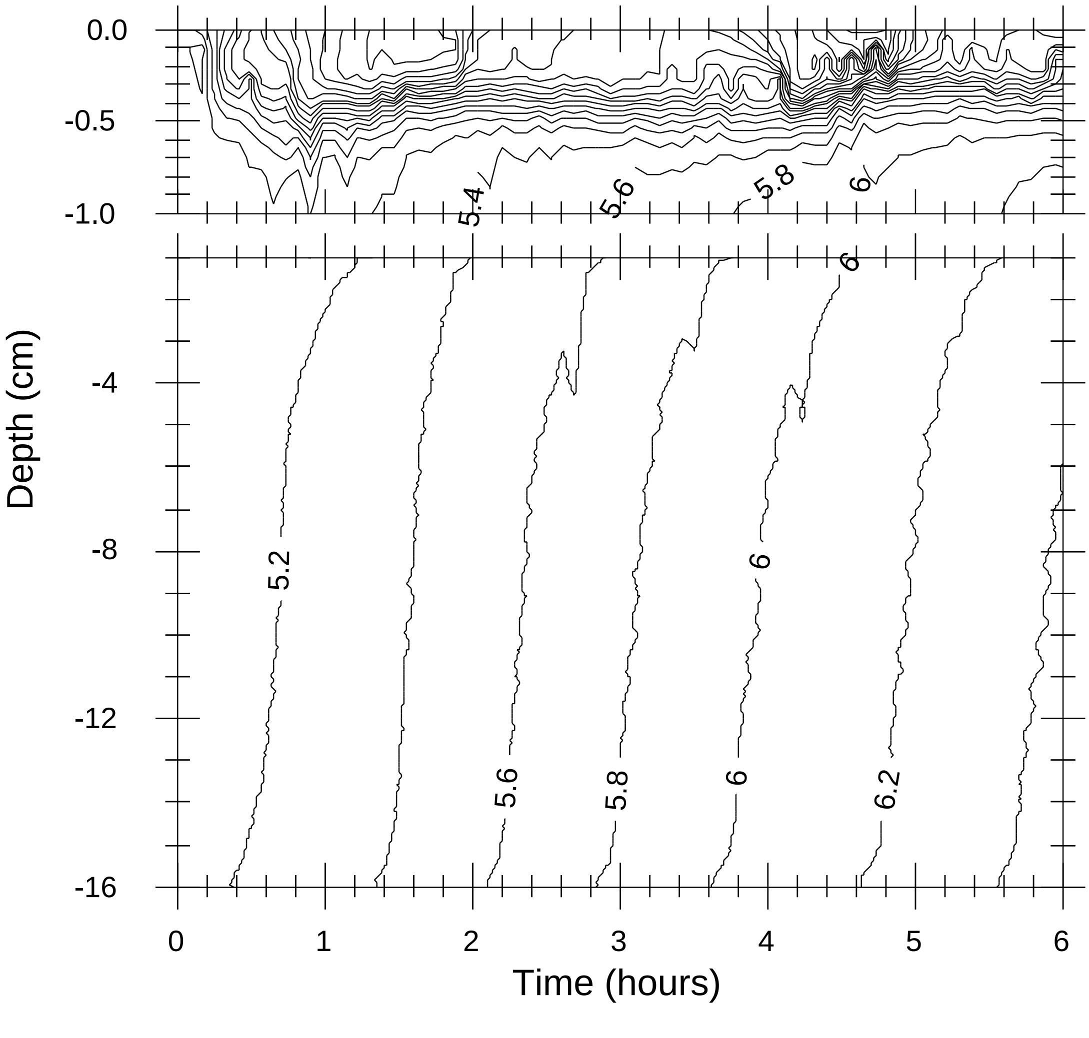

0.0
-0.5
-1.0
5.4
5.6
5.8
6
6
-4
-8
-12
-16
5.2
5.6
5.8
6
6
6.2
Depth (cm)
0
1
2
3
4
5
6
Time (hours)

Figure 2:

Blank

Figure 3:

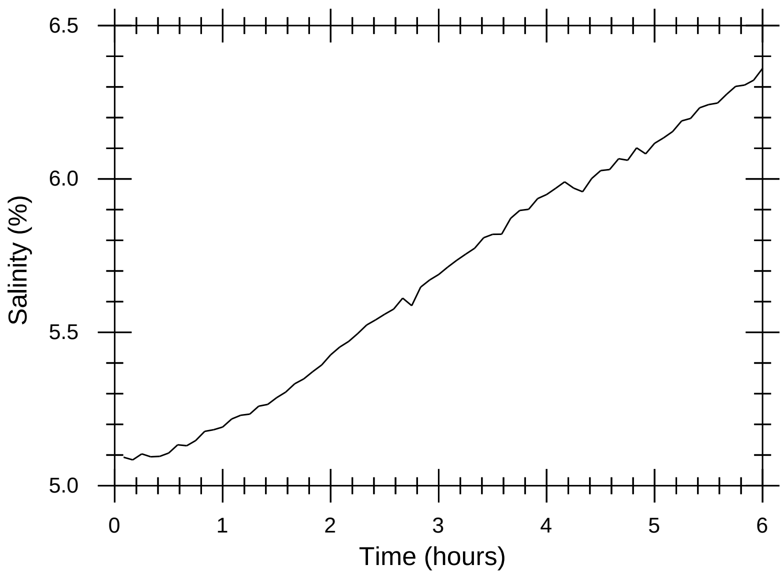

Figure 4:

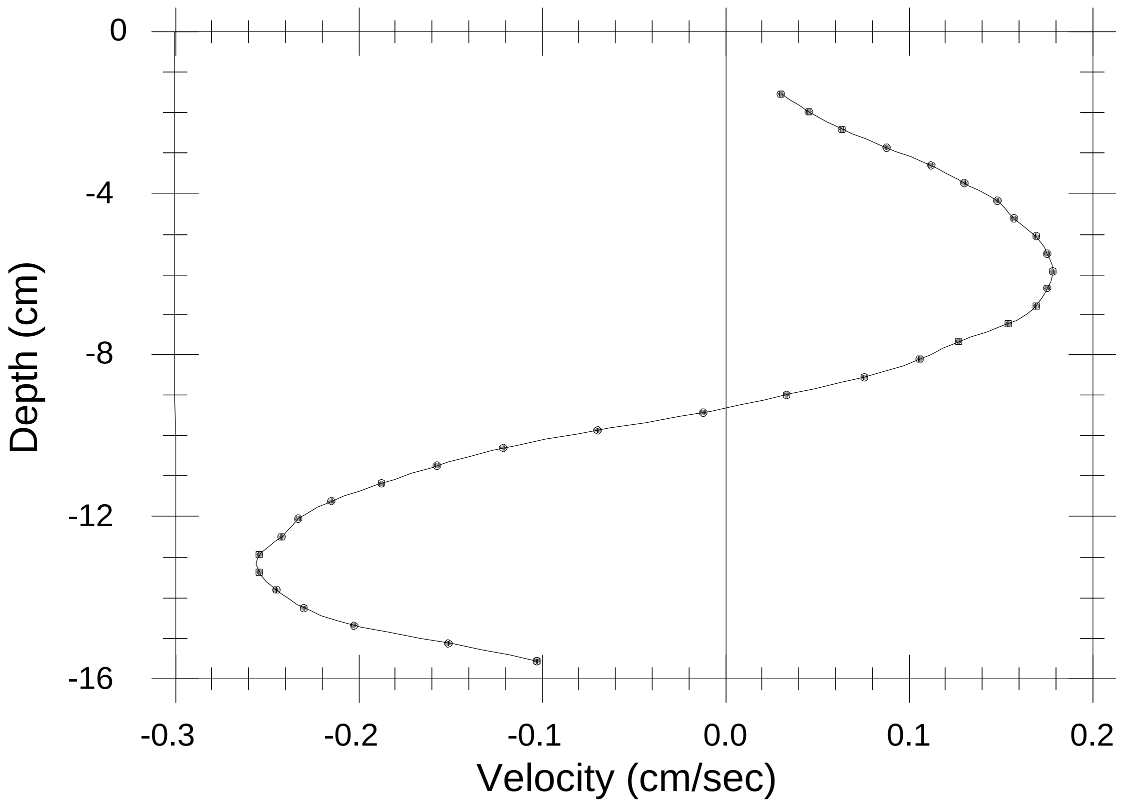

Figure 5:

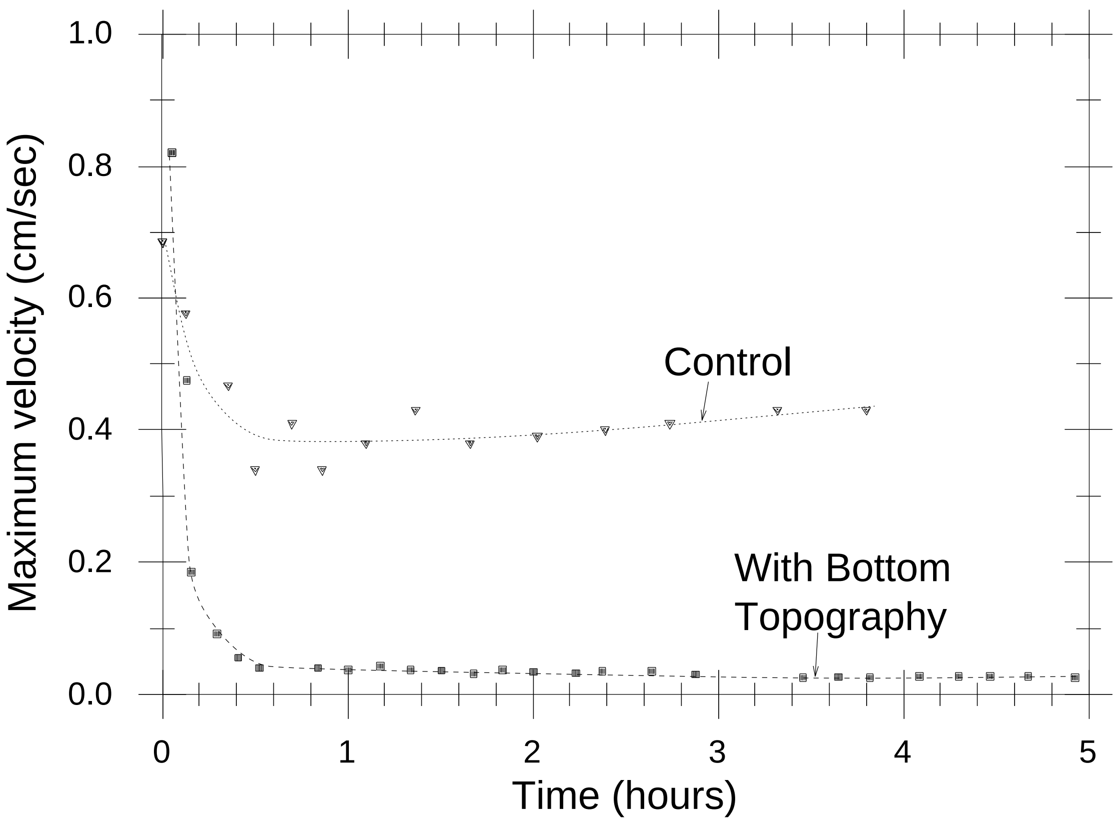
1.0
0.8
0.6
0.4
0.2
0.0
Maximum velocity (cm/sec)
0
1
2
3
4
5
Time (hours)
Control
With Bottom
Topography

Figure 6:

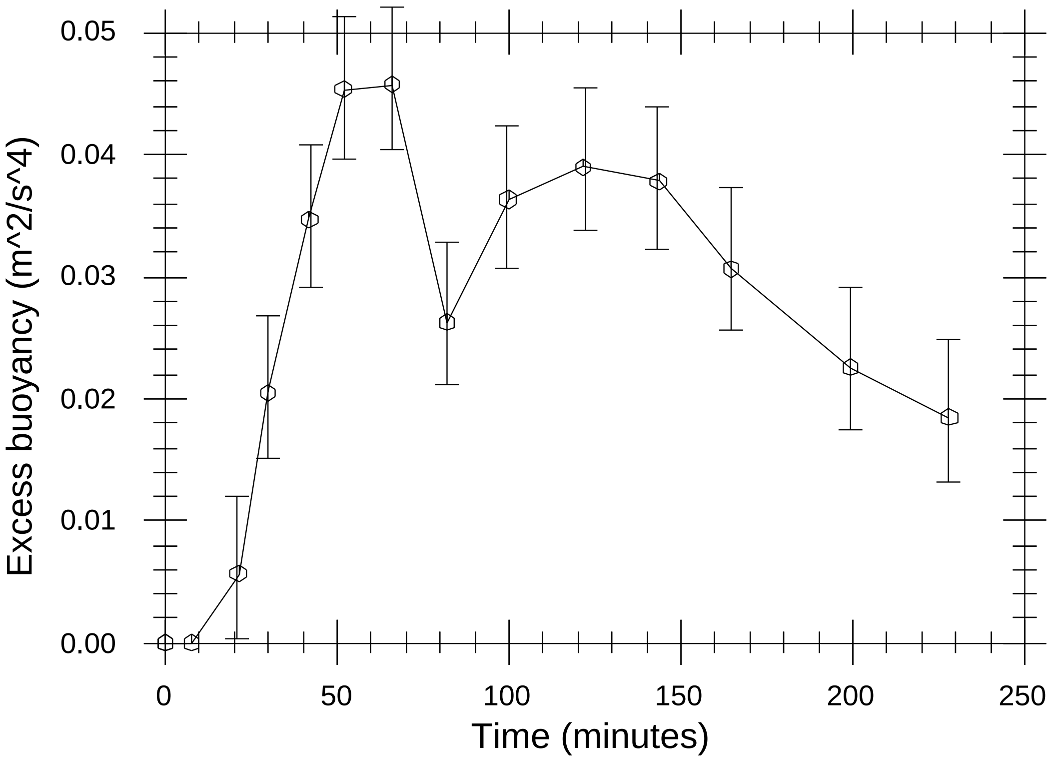
0.05
0.04
0.03
0.02
0.01
0.00
Excess buoyancy (m^2/s^4)
0
50
100
150
200
250
Time (minutes)

Figure 7:

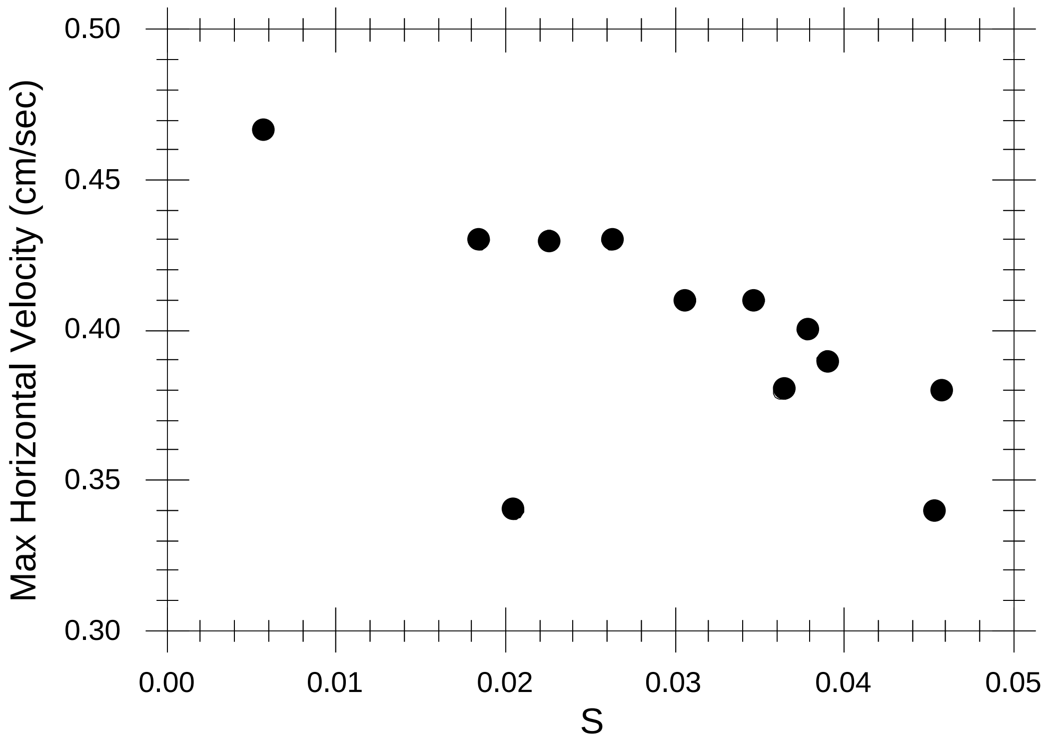

0.50
0.45
0.40
0.35
0.30
Max Horizontal Velocity (cm/sec)
0.00
0.01
0.02
0.03
0.04
0.05
S

Figure 8:

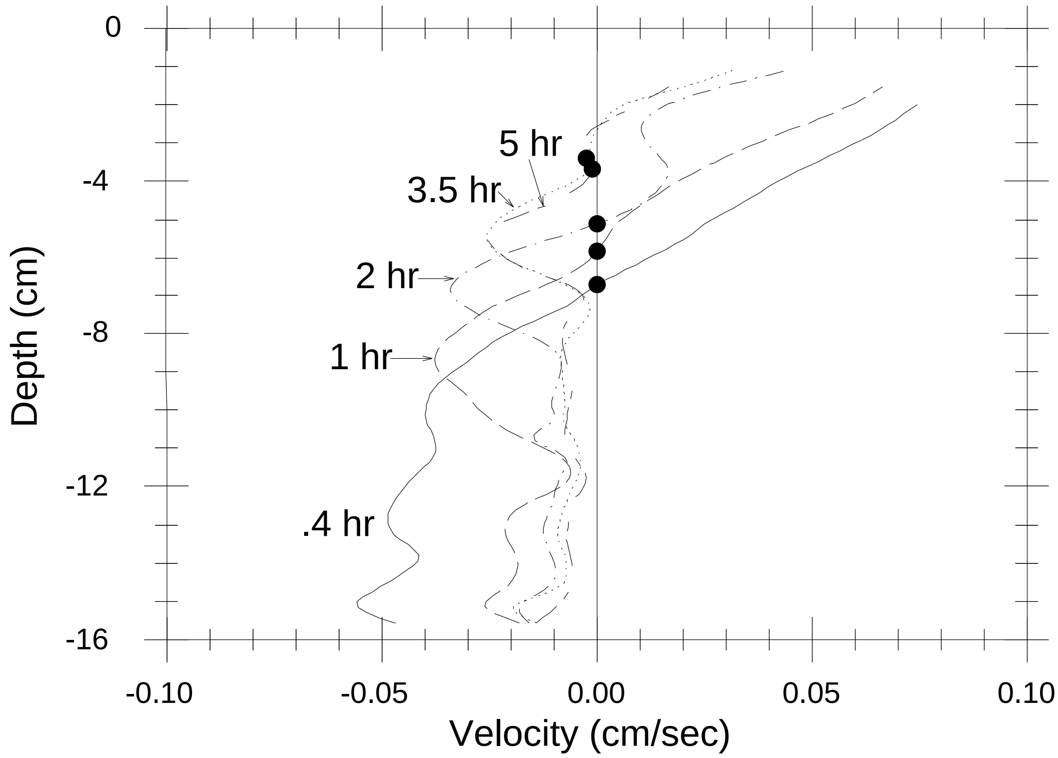

0
-4
-8
-12
-16
Depth (cm)
-0.10
-0.05
0.00
0.05
0.10
Velocity (cm/sec)
5 hr
3.5 hr
2 hr
1 hr
.4 hr

Figure 9:

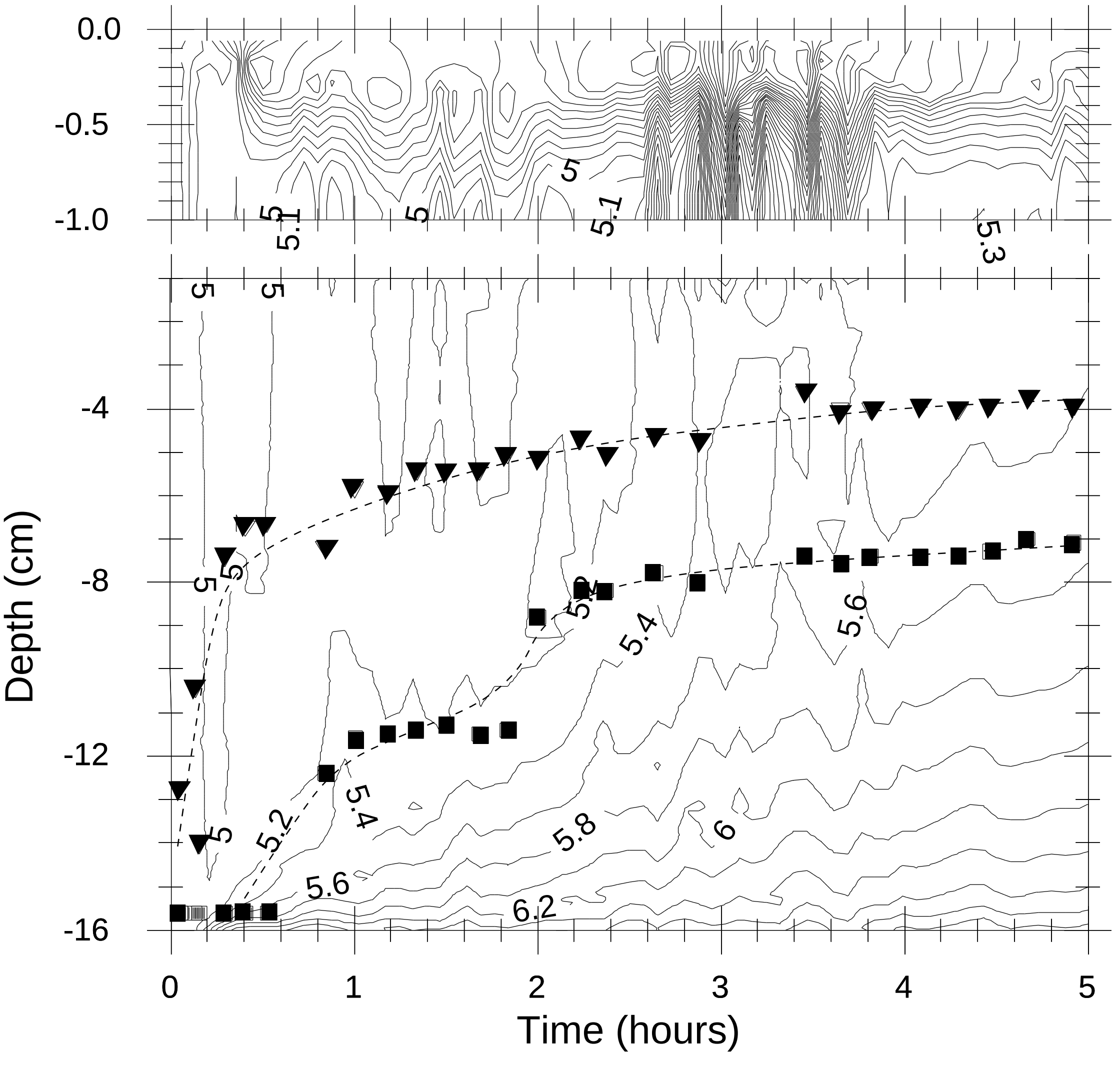

0.0
-0.5
-1.0
-4
-8
-12
-16
Depth (cm)
0
1
2
3
4
5
Time (hours)
5
5.1
5.3
5.2
5.4
5.6
5.8
6
6.2

Figure 10:

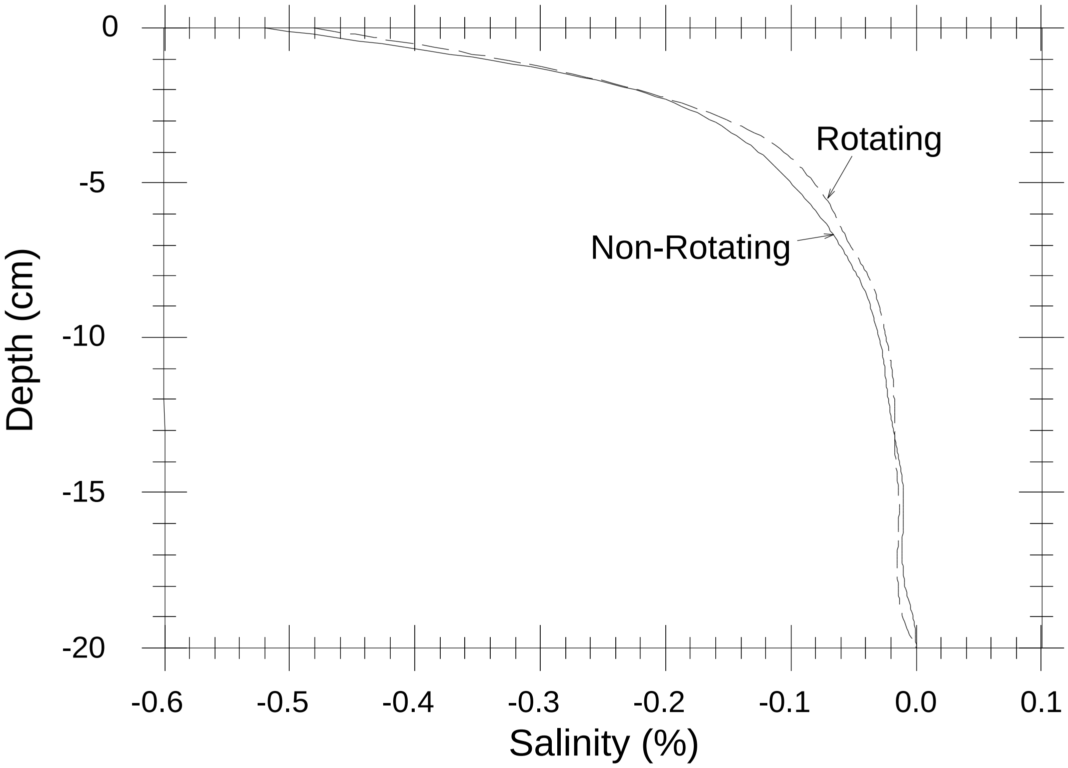

0
-5
-10
-15
-20
Depth (cm)
Rotating
Non-Rotating
-0.6
-0.5
-0.4
-0.3
-0.2
-0.1
0.0
0.1
Salinity (%)

Figure 11:

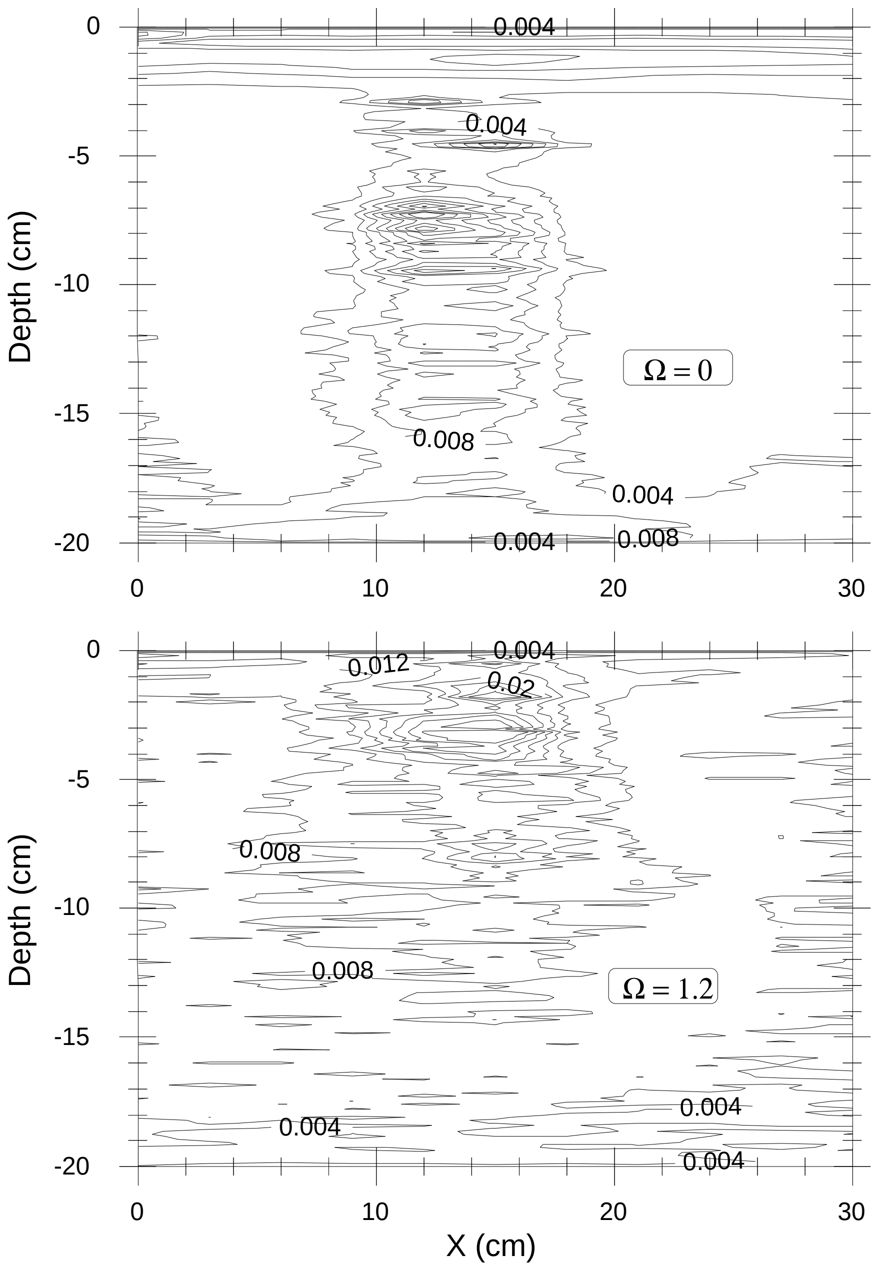

0.004
0.004
0.008
0.004
0.004
0.008
Ω = 0
Depth (cm)
0
-5
-10
-15
-20
0
10
20
30
0.004
0.012
0.02
0.008
0.008
0.004
0.004
0.004
Ω = 1.2
Depth (cm)
X (cm)

Figure 12:

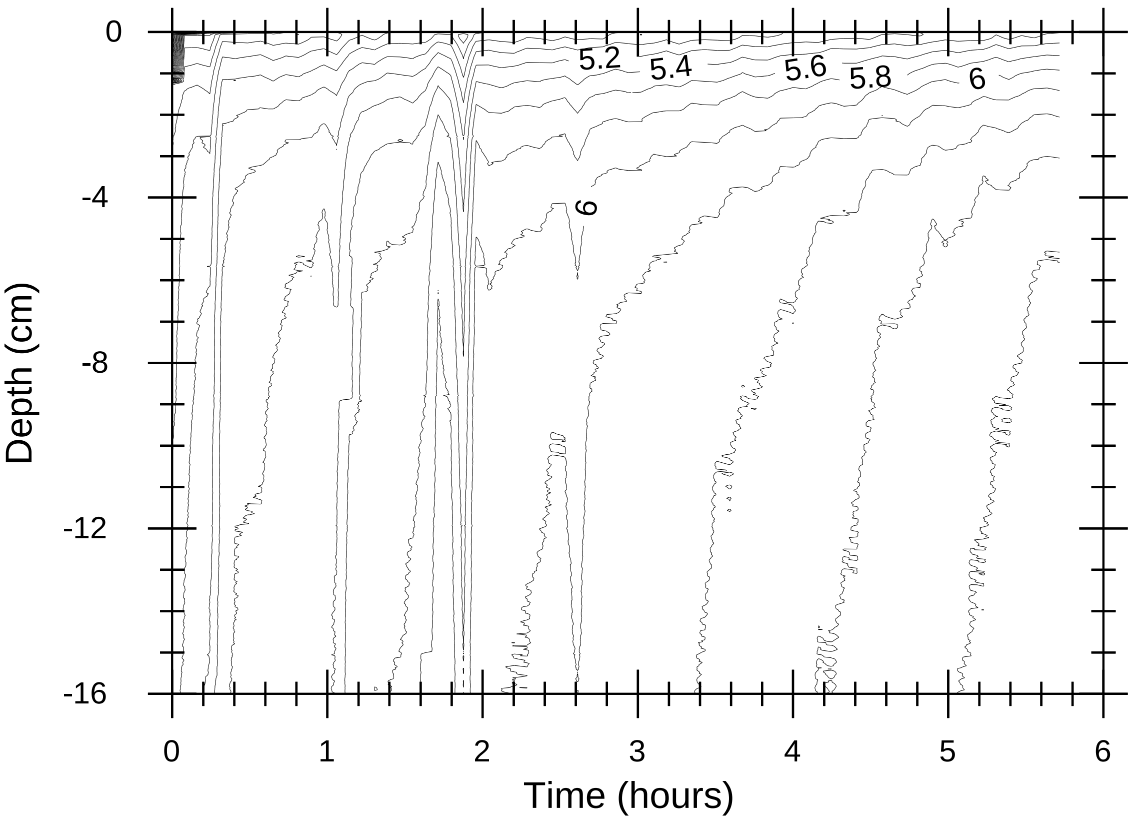

Figure 13:

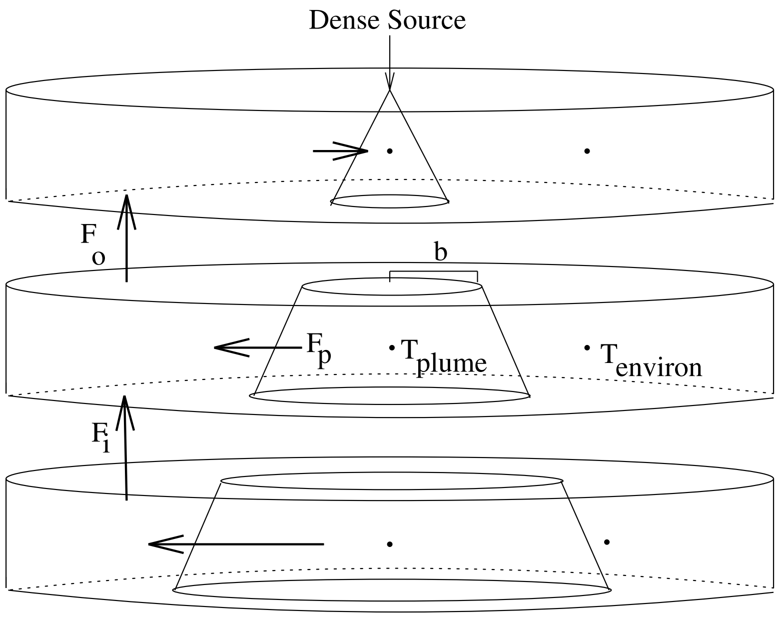

Figure 14:

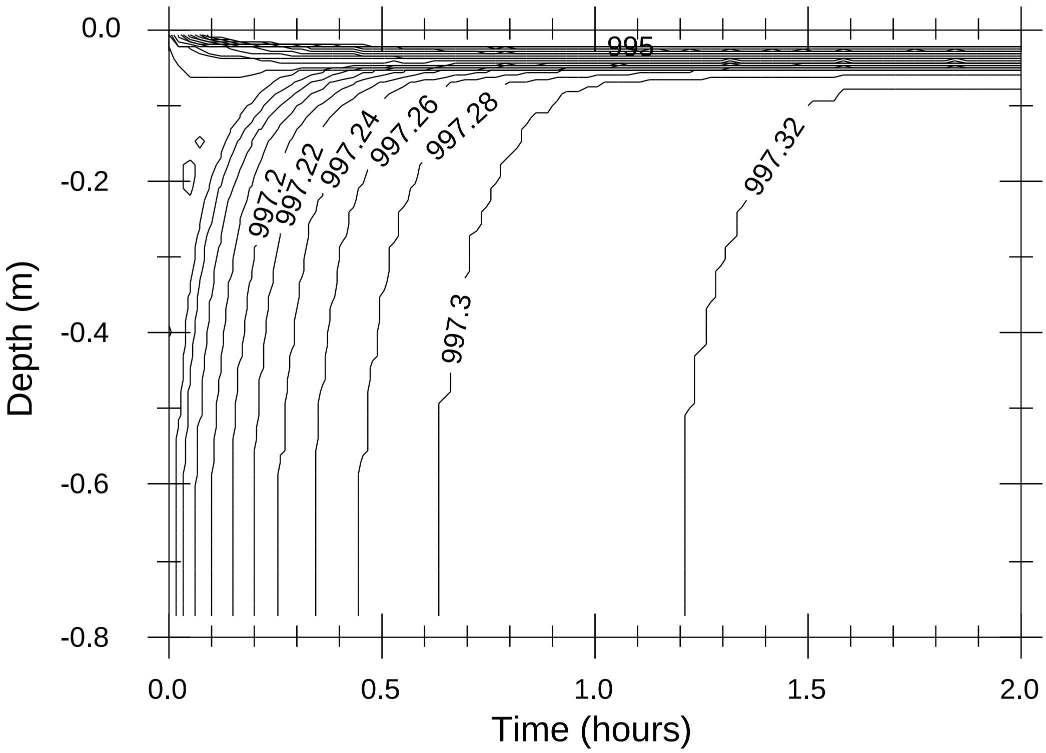

0.0
-0.2
-0.4
-0.6
-0.8
Depth (m)
0.0
0.5
1.0
1.5
2.0
Time (hours)
995
997.2
997.22
997.24
997.26
997.28
997.3
997.32

Figure 15:

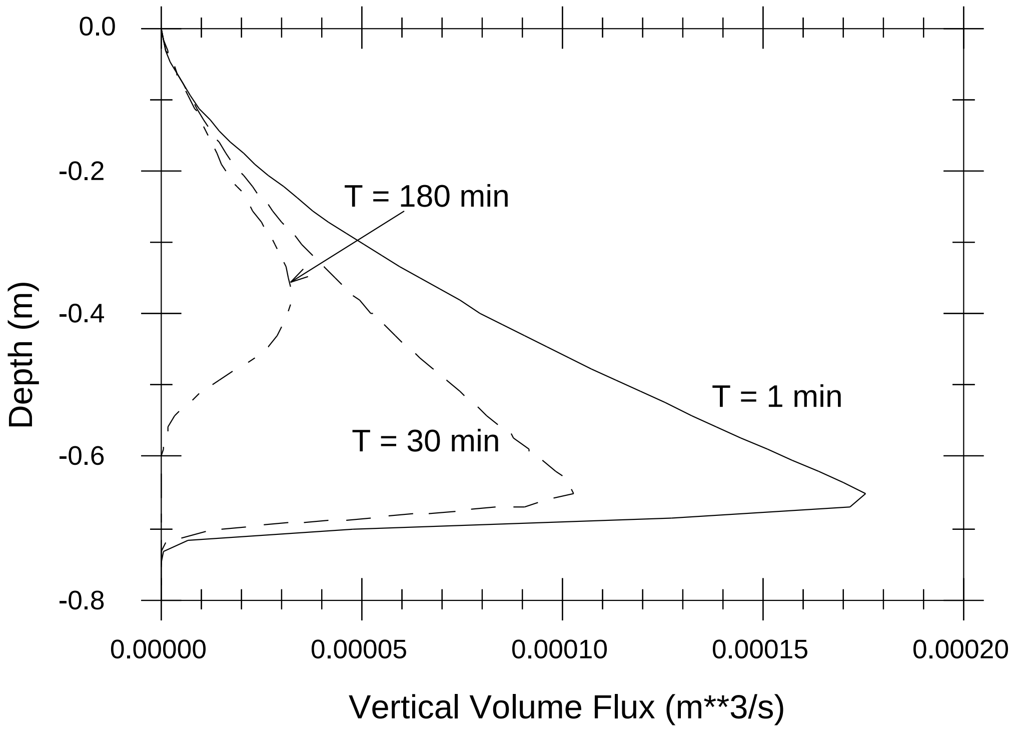
0.0
-0.2
-0.4
-0.6
-0.8
0.00000
0.00005
0.00010
0.00015
0.00020
Depth (m)
Vertical Volume Flux (m**3/s)
T = 180 min
T = 1 min
T = 30 min

Figure 16:

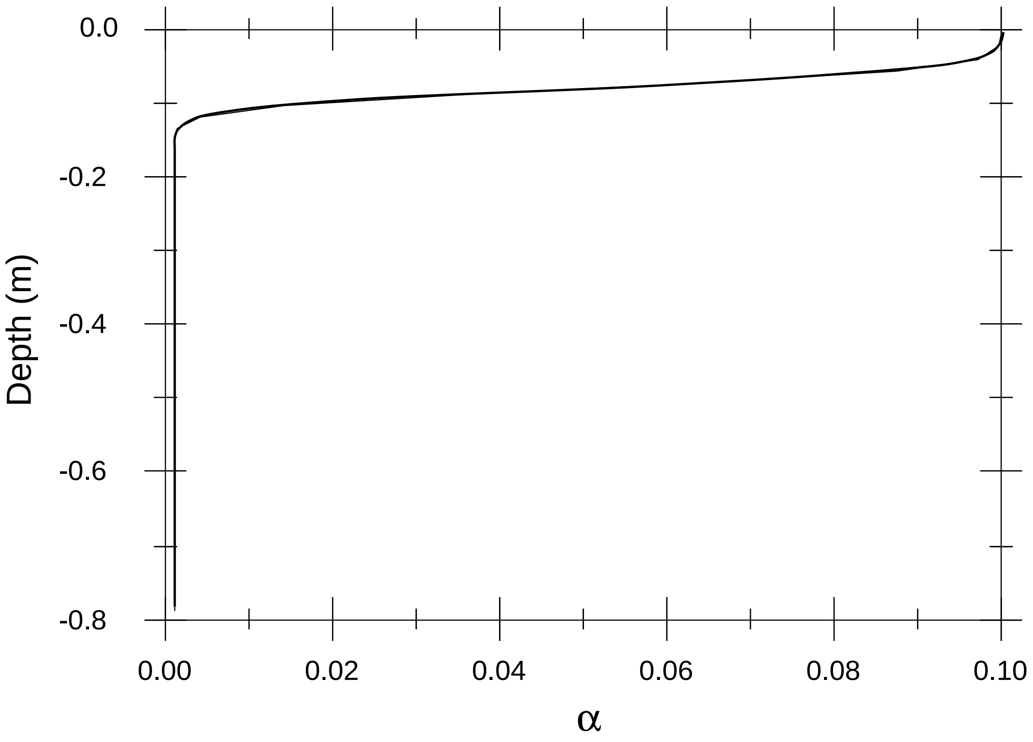

Figure 17:

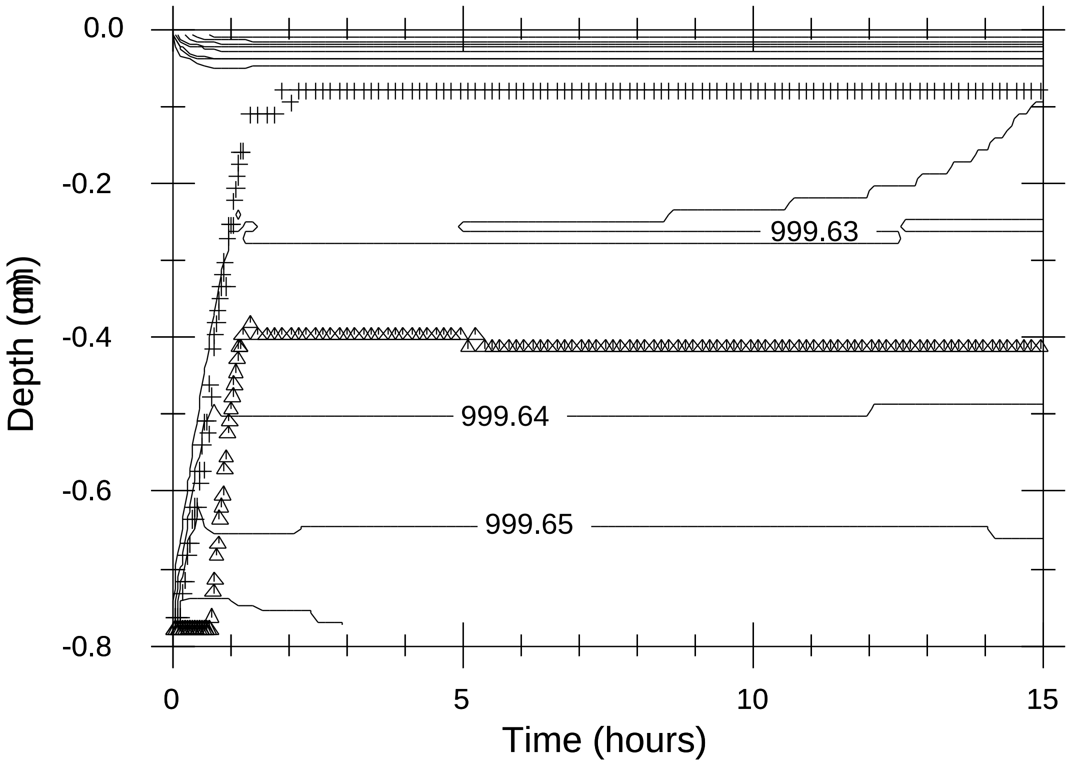

Figure 18:

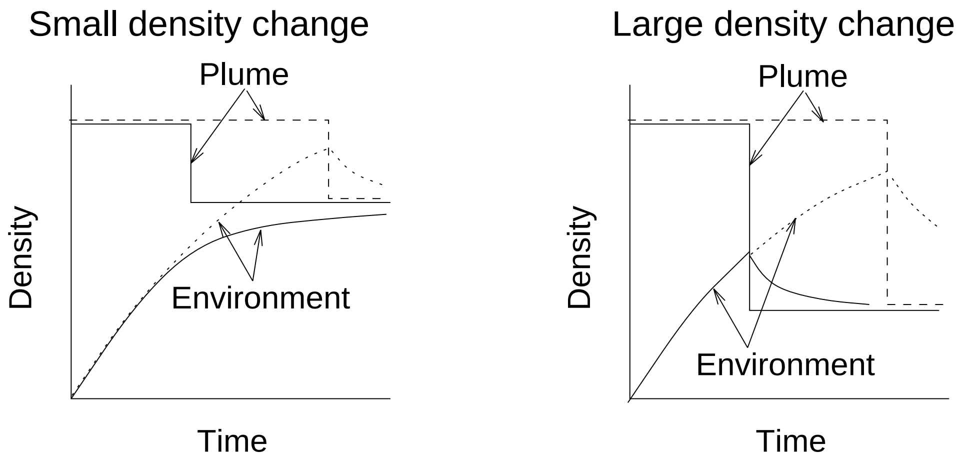
Small density change
Plume
Density
Environment
Time
Large density change
Plume
Density
Environment
Time

Figure 19: